The response of electrostatic probes via the -function

Rerup, T.O.; Crichton, George C; McAllister, Iain Wilson

Published in:
Conference Record of the 1994 IEEE International Symposium on Electrical Insulation

Link to article, DOI:
10.1109/ELINSL.1994.401461

Publication date:
1994

Document Version
Publisher's PDF, also known as Version of record

Conference Record of the 1994 IEEE International Symposium on Electrical Insulation, Pittsburgh, PA USA, June 5-8, 1994

The Response of Electrostatic Probes via the λ-Function

T.O. Rerup, G.C. Crichton and I.W. McAllister

Electric Power Engineering Department
Building 325
The Technical University of Denmark
DK-2800 Lyngby, Denmark

Abstract — The response of an electrostatic probe is examined with reference to a planar spacer. The study involves the numerical calculation of the probe λ-function, from which response-related characteristic parameters can be derived. These parameters enable the probe detection sensitivity and spatial selectivity to be quantitatively assessed. Evaluation is undertaken with reference to spacer thickness, dielectric permittivity and the proximity of the spacer to other electrodes.

INTRODUCTION

Throughout the 1980's extensive studies were undertaken on the measurement of the surface charge which accumulates at a gas/spacer interface. In an attempt to quantify such charge, the majority of experimental studies employed small electrostatic field probes to scan across the dielectric surface. Owing to mechanical requirements, each probe consists essentially of a long cylindrical shaft at earth potential, with a circular conducting disc insulated from but mounted coaxially at the end of the shaft. The potential of this disc/sensor-plate is floating. Charges are electrostatically induced on the sensor plate by the ambient surface charge, and hence as the probe is moved parallel to the surface the potential of the sensor plate changes. The probe sensor-plate potential is thus the measured parameter.

To facilitate a proper evaluation and interpretation of such probe measurements, Pedersen introduced a probe response function, the λ-function [1]. In the present study, the influence of the probe/spacer geometry and dielectric permittivity upon the λ-function is examined. Thereafter this knowledge enables the response of the probe with respect to detection sensitivity and spatial resolution to be discussed.

THE λ-FUNCTION

Pedersen's λ-function relates the charge induced on the probe to the surface charge density at the dielectric interface [1]. If it is assumed that the volume charge density within the solid dielectric is zero, then this relationship can be expressed as

$$q = -\iint_{A_0} \lambda \sigma dA \qquad (1)$$

where q is the charge induced on the sensor plate; σ is the surface charge density on the surface element dA of A_0, the surface of the solid dielectric.

In the analysis [1], the dimensionless parameter λ is shown to be a solution of the general Laplace equation for the complete measuring-system geometry: viz.

$$\vec{\nabla} \cdot (\varepsilon \vec{\nabla} \lambda) = 0 \qquad (2)$$

The boundary conditions are $\lambda = 1$ at the probe sensor-plate and $\lambda = 0$ at all other electrodes. In addition, at the dielectric interface the normal derivatives of λ must obey the condition

$$\varepsilon_+ \left(\frac{\partial \lambda}{\partial n}\right)_+ = \varepsilon_- \left(\frac{\partial \lambda}{\partial n}\right)_- \qquad (3)$$

where the + and - signs refer to the opposite sides of the interface. As (2) is just Laplace's equation, any standard method of solving this equation can be employed to evaluate the variation of λ upon the surface. On this occasion, solutions of Laplace's equation were obtained using an Ansoft finite element software package. These solutions are then utilized to study the dependence of the λ-function upon the system geometry.

SYSTEM GEOMETRY

The actual geometry of the probe system used in this study is shown in Fig.1a, in which r is the radius of the sensor plate and x is the radial distance from the probe axis. The outer radius of the probe guard ring is R, while the gap between the sensor plate and the guard ring is Δ. To minimize the influence on λ of the probe shaft of length L, this latter parameter was made as large as possible. In the present case L was set to be greater than $90r$. The probe is positioned perpendicular to a planar dielectric surface, at a height h above the gas/dielectric interface.

The dielectric spacer, of relative permittivity ε_r, has a thickness t in a direction parallel to the probe axis, while positioned at a distance d beneath this dielectric slab is a parallel plane conducting boundary; see Fig.1b. In the direction normal to the probe axis, the extent of the solid dielectric is much greater than the outer diameter of the probe. With the present software, this distance is set to $250r$.

RESULTS AND DISCUSSION

We will consider the influence of the dielectric geometry upon λ. With respect to the probe itself, the dimensions originally employed by Pedersen are used [1]: i.e. $R = 6r$, $\Delta = 0.1r$ and $h = 0.5r$.

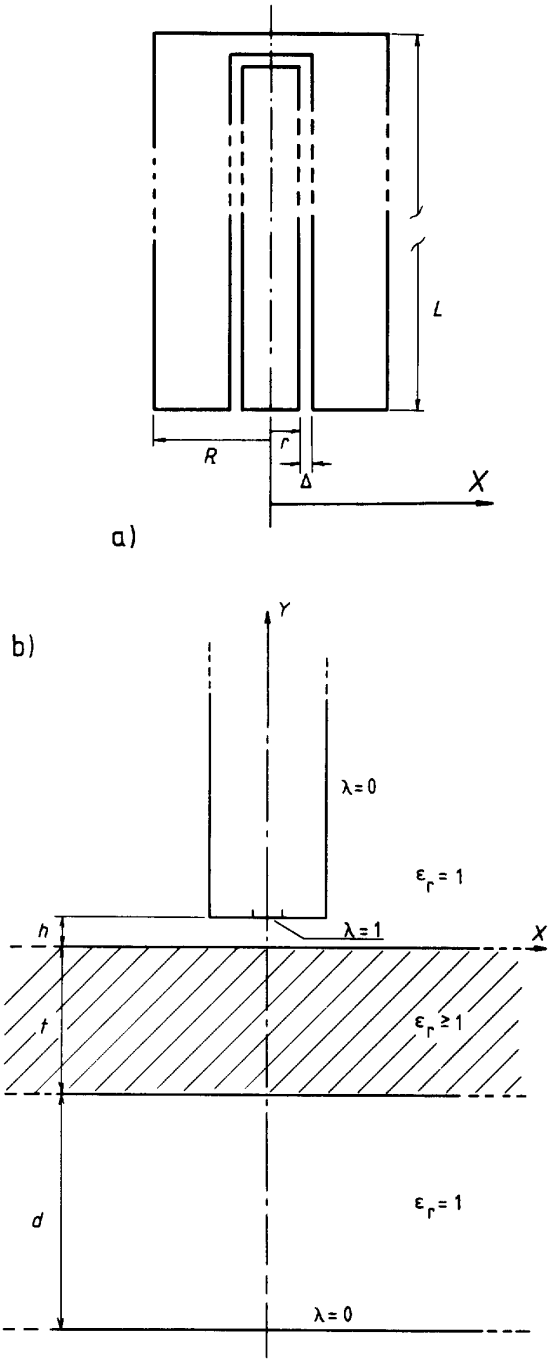

Figure 1. The system geometry.

Finite t, d → ∞

For this condition, we have two gas/solid dielectric interfaces. To distinguish between these, we will identify the near interface with the subscript 'n' and the far interface with the subscript 'f'.

The Near Interface: The variation of λ_n along the near interface is illustrated in Fig.2 for $t = 100r$, and $1 \leq \varepsilon_r \leq 6$. For increasing ε_r-values a marked reduction in $\lambda_n(0)$ is observed, see Fig.2a, while the opposite trend is to be seen for $x \geq R$, see Fig.2b. From these diagrams it is clear that the λ_n-distribution can be related to two regions. In this context, it is useful to let λ_{ni} denote the λ_n-function *within* the area subtended by the probe; i.e. for $0 \leq x \leq R$. In the same manner, we let λ_{no} denote the λ_n-function *outwith* the area subtended by the probe; i.e. for $x \geq R$.

Similar calculations for $t = 10r$ and $t = r$ produced essentially the same $\lambda_n(x)$ variations: see Table 1.

Although the λ_{no}-values may appear to be insignificant in relation to the λ_{ni}-values, it should be borne in mind that this is not the complete picture with respect to induced-charge magnitudes.

If (x,y) represent cylindrical coordinates, see Fig.1b, then for a disc of constant surface charge density σ_o located at a dielectric interface, the induced charge q on the sensor plate is given by

$$q(x) = 2\pi\sigma_o \int_0^x \lambda(x',y)x'dx' \qquad (4)$$

where x' is a dummy variable, and a constant y represents a planar interface. In discussing the variation of $q(x)$, it proves convenient to introduce a detection sensitivity $S_e(x)$ defined by

$$S_e(x) = (2/r^2) \int_0^x \lambda(x',y)x'dx' \qquad (5)$$

The value of $S_{en}(x)$ for specific x-values are listed in Table 2, columns 2 and 3. Owing to the product $\lambda(x,y)x$ in (5), the large variation in $\lambda_n(0)$-values with ε_r is not reflected in the $S_{en}(R)$-values.

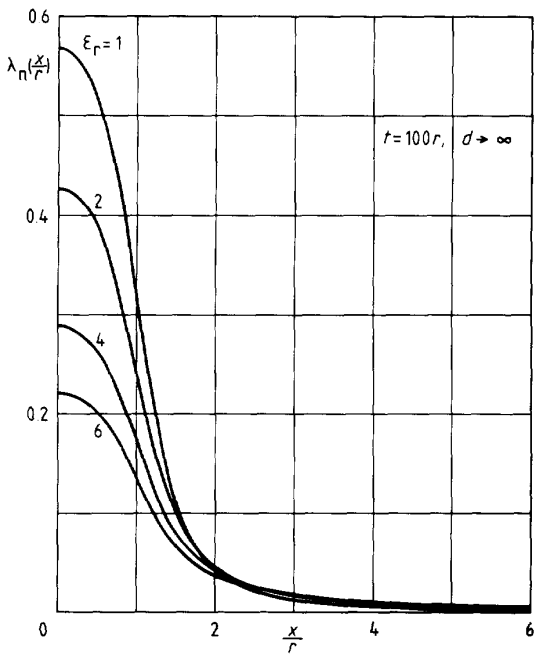

Figure 2a. Variation of $\lambda_n(x)$, $0 \leq x \leq 6r$.

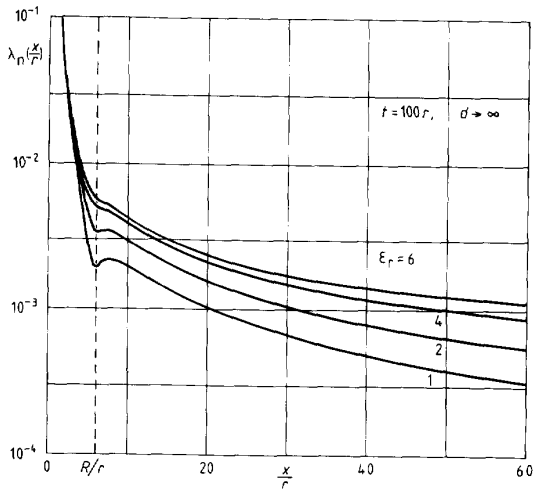

Figure 2b. Variation of $\lambda_n(x)$, $0 \leq x \leq 60r$.

Table 1: $\lambda_n(x)$ data for $d \to \infty$.

t/r	100	10	1
ε_r	$\lambda_n(0)$	$\lambda_n(0)$	$\lambda_n(0)$
1	0.570	0.570	0.570
2	0.427	0.427	0.442
4	0.289	0.289	0.316
6	0.220	0.220	0.251
ε_r	$\lambda_n(R)$	$\lambda_n(R)$	$\lambda_n(R)$
1	1.93(-3)	1.93(-3)	1.93(-3)
2	3.38(-3)	3.55(-3)	2.88(-3)
4	4.99(-3)	5.66(-3)	4.50(-3)
6	5.67(-3)	6.57(-3)	5.84(-3)
ε_r	$\lambda_n(10R)$	$\lambda_n(10R)$	$\lambda_n(10R)$
1	3.19(-4)	3.08(-4)	3.08(-4)
2	5.52(-4)	5.78(-4)	3.41(-4)
4	8.89(-4)	1.03(-3)	4.06(-4)
6	1.12(-3)	1.38(-3)	4.80(-4)

Note (-3) ≡ 10^{-3}

Table 3: $\lambda_f(x)$ data for $d \to \infty$.

t/r	100	10	1
ε_r	$\lambda_f(0)$	$\lambda_f(0)$	$\lambda_f(0)$
1	2.28(-4)	5.75(-3)	0.181
2	4.47(-4)	7.45(-3)	0.183
4	7.81(-4)	8.59(-3)	0.159
6	1.02(-3)	8.84(-3)	0.138
ε_r	$\lambda_f(R)$	$\lambda_f(R)$	$\lambda_f(R)$
1	2.27(-4)	4.09(-3)	4.44(-3)
2	4.46(-4)	5.53(-3)	4.61(-3)
4	7.80(-4)	6.74(-3)	5.68(-3)
6	1.02(-3)	7.18(-3)	6.78(-3)
ε_r	$\lambda_f(10R)$	$\lambda_f(10R)$	$\lambda_f(10R)$
1	1.87(-4)	3.22(-4)	3.10(-4)
2	3.80(-4)	5.89(-4)	3.42(-4)
4	6.91(-4)	1.04(-3)	4.07(-4)
6	9.23(-4)	1.38(-3)	4.80(-4)

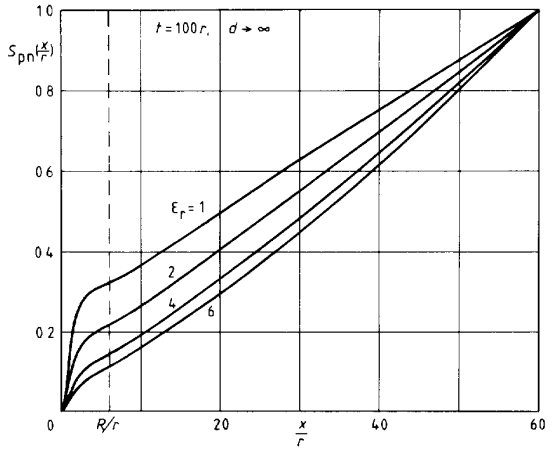

Figure 3. Variation of $S_{pn}(x)$ for $t = 100r$ and $d \to \infty$.

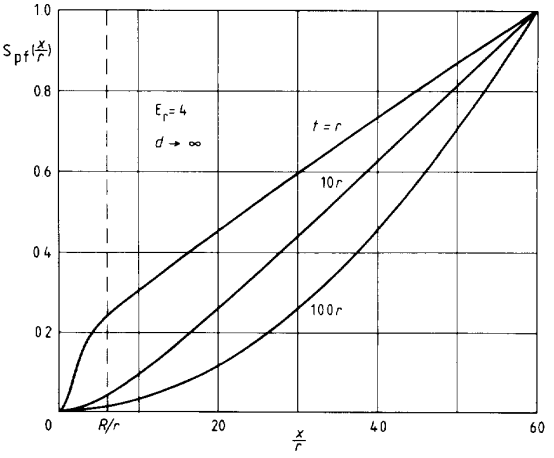

Figure 4. Variation of $S_{pf}(x)$ for $\varepsilon_r = 4$ and $d \to \infty$.

Table 2: $S_e(x)$ data for $d \to \infty$ and $d = 0$.

		$t/r = 100$, $d \to \infty$			$t/r = 100$, $d \to 0$	
ε_r	$S_{en}(R)$	$S_{en}(10R)$	$S_{ef}(R)$	$S_{ef}(10R)$	$S_{en}(R)$	$S_{en}(10R)$
1	1.013	3.136	0.008	0.739	1.012	2.879
2	0.941	4.329	0.016	1.478	0.940	3.621
4	0.825	5.724	0.028	2.636	0.821	4.116
6	0.737	6.511	0.037	3.482	0.728	4.135
		$t/r = 10$, $d \to \infty$			$t/r = 10$, $d \to 0$	
ε_r	$S_{en}(R)$	$S_{en}(10R)$	$S_{ef}(R)$	$S_{ef}(10R)$	$S_{en}(R)$	$S_{en}(10R)$
1	1.013	3.101	0.174	2.607	1.004	1.347
2	0.946	4.737	0.230	4.299	0.923	1.371
4	0.842	7.109	0.272	6.721	0.790	1.303
6	0.764	8.665	0.285	8.309	0.688	1.201
		$t/r = 1$, $d \to \infty$			$t/r = 1$, $d \to 0$	
ε_r	$S_{en}(R)$	$S_{en}(10R)$	$S_{ef}(R)$	$S_{ef}(10R)$	$S_{en}(R)$	$S_{en}(10R)$
1	1.013	3.100	0.848	3.050	0.730	0.730
2	0.999	3.343	0.970	3.316	0.548	0.548
4	0.974	3.809	0.920	3.793	0.365	0.365
6	0.948	4.327	0.908	4.315	0.274	0.274

The transition in the $[\lambda_n(x),x]$-curves with ε_r is however reflected in the $S_{en}(x)$-values; *viz.* the $S_{en}(R)$-values decrease with increasing ε_r, while the opposite is the case for $S_{en}(10R)$. The effect of the dielectric thickness upon λ_n is also reflected in the S_{en}-values.

With respect to $q(x)$, we can also define a spatial selectivity factor $S_p(x)$ given as

$$S_p(x) = \frac{\int_0^x \lambda(x')x'dx'}{\int_0^{x_o} \lambda(x')x'dx'} \qquad (6)$$

where x_o is the maximum radial extent of the charged area. In this study $x_o = 10R$. The parameter x_o allows the spatial selectivity of the probe to be quantified. The variations of $S_{pn}(x)$ for the λ_n functions of Fig.2 are shown in Fig.3. From this diagram it is evident that, for a large area of charge, λ_{no} can contribute a major portion of the recorded signal. Such a situation arises owing to the extent of the charged area relative to the probe dimensions. Similar $S_{pn}(x)$ variations are obtained with $t = 10r$ and $t = r$.

The Far Interface: With reference to the far interface, the variation of λ_f exhibits features which differ from those

Table 4: $\lambda_n(x)$ data for $d = 0$.

t/r	100	10	1
ε_r	$\lambda_n(0)$	$\lambda_n(0)$	$\lambda_n(0)$
1	0.570	0.569	0.526
2	0.427	0.427	0.375
4	0.289	0.288	0.239
6	0.220	0.219	0.175
ε_r	$\lambda_n(R)$	$\lambda_n(R)$	$\lambda_n(R)$
1	1.92(-3)	1.60(-3)	3.01(-6)
2	3.34(-3)	2.70(-3)	5.51(-6)
4	4.84(-3)	3.78(-3)	7.13(-6)
6	5.38(-3)	4.10(-3)	7.03(-6)
ε_r	$\lambda_n(10R)$	$\lambda_n(10R)$	$\lambda_n(10R)$
1	2.39(-4)	5.83(-6)	7.79(-12)
2	3.37(-4)	4.13(-6)	5.55(-12)
4	4.08(-4)	2.53(-6)	3.07(-12)
6	4.19(-4)	1.78(-6)	1.90(-12)

of λ_n. As could be expected, λ_{fi} is very dependent on the thickness of the dielectric, and in addition $\lambda_f(0)$ increases with increasing ε_r, see Table 3. For $t = 100r$, λ_f is essentially constant, while for $t = r$, λ_f exhibits a peaked variation similar to that of λ_n.

These λ_f features are reflected in the $S_{ef}(R)$-values, see Table 2, columns 4 & 5, in that the $S_{ef}(R)$ contribution to the probe signal increases with reduction in dielectric thickness. The magnitude of $S_{ef}(10R)$ is also influenced by the dielectric thickness, but not to the same degree as $S_{ef}(R)$. The λ_f characteristics are also evident in the variations of $S_f(x)$, see Fig.4. For $t = r$, $S_{pf}(x)$ is similar to $S_{pn}(x)$, cf. Fig.4 with Fig.3. However owing to the lack of a distinctive peak in λ_{fi}, the form of $S_{pf}(x)$ for $t = 10r$ and $t = 100r$ is quite different; i.e. $\lambda_{fi}(x)$ now contributes < 5% to the probe signal.

Finite t, d = 0

Owing to the λ-function boundary conditions, the existence of the plane electrode ensures that $\lambda_f = 0$, and thus we have only the variation of λ_n to consider.

For $t = 100r$, the influence of having $d = 0$ is minimal, cf. Table 4 with Table 1. However upon reducing the dielectric thickness to $10r$ and thereafter to r, the influence of the plane conductor becomes evident in that λ_{no} is reduced by several orders of magnitude, see Tables 4 and 1. The significance of this reduction is best indicated by the corresponding variations of $S_{pn}(x)$, which are shown in Fig.5, for $\varepsilon_r = 4$ and for various values of t. As t is reduced, there is a gradual transition from $t = 100r$, for which λ_{no} contributes > 80% of the recorded signal, to $t = r$ where λ_{no} contributes < 0.1%. A consequence of this increase in spatial selectivity is that the magnitude of the associated $S_{en}(10R)$ decreases by an order of magnitude, although the reduction in $S_{en}(R)$ is less: Table 2 columns 6 & 7.

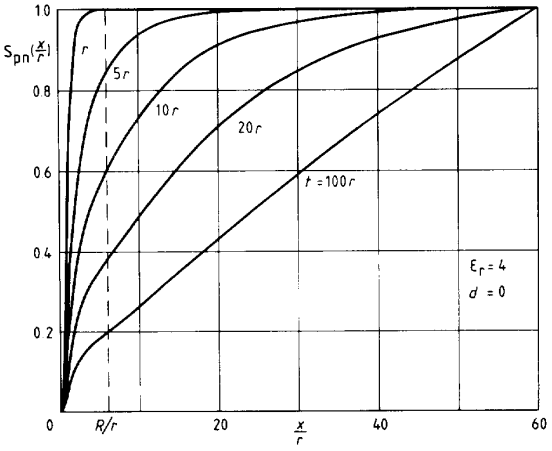

Figure 5. Variation of $S_{pn}(x)$ for $\varepsilon_r = 4$ and $d = 0$.

CONCLUSION

An examination of a probe λ-function associated with a planar dielectric body has indicated that contributions to the induced-charge from areas outwith that immediately subtended by the probe can account for a major portion of the probe signal. Moreover, the interpretation and evaluation of the probe signal can become still further complicated by the presence of a second charged interface. However, the study indicates that, for thin planar specimens, the spatial selectivity of the probe response can be optimised with the provision of a local $\lambda = 0$ electrode boundary, the effect of which is to suppress the induced-charge contributions from less immediate areas and/or far interfaces of the dielectric body.

REFERENCES

[1] A.Pedersen, "On the Electrostatics of Probe Measurements of Surface Charge Densities" in L.G. Christophorou and D.W. Bouldin, *Gaseous Dielectrics V*. New York: Pergamon Press, 1987,pp.235-240.